Deformation and Damage of Random Fibrous Networks

Emrah Sozumert , Farukh Farukh , Baris Sabuncuoglu , Emrah Demirci , Memis Acar , Behnam Pourdeyhimi , Vadim V. Silberschmidt

PII: S0020-7683(18)30501-8
DOI: https://doi.org/10.1016/j.ijsolstr.2018.12.012
Reference: SAS 10211

To appear in: *International Journal of Solids and Structures*

Received date: 21 September 2018
Revised date: 22 November 2018

Please cite this article as: Emrah Sozumert , Farukh Farukh , Baris Sabuncuoglu , Emrah Demirci , Memis Acar , Behnam Pourdeyhimi , Vadim V. Silberschmidt , Deformation and Damage of Random Fibrous Networks, *International Journal of Solids and Structures* (2018), doi: https://doi.org/10.1016/j.ijsolstr.2018.12.012

HIGHLIGHTS

- Damage and fracture mechanisms of fibrous networks are investigated.
- A combined experimental and numerical (finite-element) study is implemented.
- Effects of notch shape on deformation localization and damage evolution are studied.
- A notch in fibrous networks does not cause a significant increase in localized strain.

Deformation and Damage of Random Fibrous Networks

Emrah Sozumert[a], Farukh Farukh[b], Baris Sabuncuoglu[c], Emrah Demirci[a],

Memis Acar[a], Behnam Pourdeyhimi[d], Vadim V. Silberschmidt[a,1]

[a]*Wolfson School of Mechanical, Electrical and Manufacturing Engineering, Loughborough University, Leicestershire, UK*

[b]*School of Engineering and Sustainable Development, De Montfort University, Leicestershire, UK*

[c]*Mechanical Engineering, Hacettepe University, Ankara, Turkey*

[d]*The Nonwovens Institute, North Carolina State University, Raleigh, NC, USA*

Abstract

Fibrous networks are encountered in various natural and synthetic materials. Typically, they have random microstructures with complex patterns of fibre distribution. This microstructure, together with significant (in many cases) stretchability of such networks, results in a non-trivial load-transfer mechanism, different from that of continuous media. The aim of this study is to investigate evolution of local deformation, damage and fracture processes in fibrous networks. In order to do this, together with extensive experiments, discontinuous finite-element (FE) models with direct incorporation of microstructural features were developed using a parametric approach for specimens with various dimensions and different types of notches. These models, mimicking a microstructure of the selected fibrous network, were loaded by stretching along a principal direction. Discontinuous FE models provided data not only on a global response of the specimens but also on levels of stresses and strains in each fibre, forming the network. An effect of a notch shape on evolution of fibre strains as well as mechanisms and patterns of damage was investigated using experimental data and simulation results, assessing also toughness of specimens. Strain distribution over selected paths were tracked in notched specimens to quantify strain distributions in the vicinity of notch tips. The growth and patterns of local damage due to axial stretching obtained in advanced numerical

[1] Corresponding author (Vadim V. Silberschmidt): Wolfson School of Mechanical, Electrical and Manufacturing Engineering, Loughborough University, Ashby Road, Loughborough, Leics., LE11 3TU, UK
Email address: V.Silberschmidt@lboro.ac.uk

simulations with the developed FE models demonstrated a good agreement with experimental observations.

Keywords: Fibrous materials; notch sensitivity; deformation and damage; mechanics of fibrous materials; finite-element modelling; orientation distribution

1. Introduction

Fibrous networks are ubiquitous in many natural materials, such as bone tissues, skin [1], wood [2] and bacterial cellulose [3], as well as artificial ones, such as polymer-based nonwovens. In many cases, mechanical response of such fibrous networks can be tuned by controlling their microstructure [4]. Therefore, mechanical performance of such networks is of interest for researchers due to a broad range of potential applications. Nonwovens are a suitable example to study these materials. They are fibrous materials formed by short or long fibres bonded together by various web-bonding techniques such as mechanical or chemical bonding or heat treatment. Unlike woven materials, nonwovens are disordered as a result of their manufacturing, and they demonstrate anisotropy in three main orthogonal directions: machine direction (MD), cross direction (CD) and thickness direction (TD). The character of distribution of constituent fibres in nonwoven materials depends on the type of the manufacturing process; the non-uniformity of their orientational distribution defines an anisotropy of their mechanical behaviour. For instance, thermally bonded calendered nonwoven webs exhibit very low stiffness in CD and TD compared to that in MD [5-7] since fibres are preferentially aligned along the machine direction. To characterise the random fibre orientation, a distribution function was introduced by Cox in 1952 [8]. Fourier- or Hough-transform-based methods were employed to improve the accuracy of assessment of this orientation distribution function [5, 9, 10].

Several studies based on experimental analysis and numerical modelling related to deformation and fracture of nonwovens were performed, some focusing on micro-mechanisms underpinning these phenomena [11-17]. Numerical methods can also be used to asses stiffness of fibres in biomaterials [18]. 3D X-Ray images can be processed to extract complex morphological features such as tortuosity in random fibrous networks [19]. Effective thermal and elastic properties were estimated from homogenisation over hundreds of representative volume elements (RVEs) [20]. Generally, in fibrous materials, damage is

initiated by debonding of fibres under low levels of strain followed by their re-orientation in the direction of loading [21]; straightening of fibres and re-orientation trigger the damage mechanisms at advanced stages of stretching [22]. Progressive failure of the fibres that reach a stress (or a strain) threshold results in a development of localised failure zones; growth of these zones leads to a final rupture of a fibrous web [22]. Spatial non-uniformity of fibrous networks causes variations in localisation of strain and failure [23]. A specific microstructure of nonwovens can even enhance tensile strength in presence of a notch [24]. To the authors' knowledge, only limited research pertaining to micro-mechanisms and mechanical behaviour of fibrous materials containing localised damage is available in the literature. Such local damage is very important for structural integrity of the material, and its effects on materials behaviour can be assessed in terms of notch sensitivity. A better understanding of these mechanisms is vital for elucidation of properties and performance of fibrous materials in numerical models.

In this research, to assess the effect of notches on deformation and damage characteristics of fibrous materials, a special type of nonwoven was chosen as an example of a fibrous network. The focus is on the influence of notch geometry and sample size on deformation and damage mechanisms in disordered fibrous materials. To achieve this, various notch geometries in a polymer-based nonwoven material are studied using a combination of experimental tests and advanced numerical analysis. This study extends analysis of various types of damage in fibrous materials performed by other researchers. For instance, in a polypropylene nonwoven networks, a complete blunting of a central slit occurred reducing stress concentration around it, where the damage was localized. This mechanism is entirely different in the nonwoven composed of brittle fibres, resulting in the load transfer in fibre bundles from a crack tip to out-of-notch regions [12, 13, 21], leading to distribution of stresses to a larger area, reducing notch sensitivity. Rawal et al. [16] conducted an experimental research on needle-punched hybrid nonwovens composed of polypropylene and viscous fibres in various ratios and considered the effect of circular and longitudinal notches on micro-mechanisms of deformation and damage. It was reported that the circular notches were more detrimental than a longitudinal cut; however, a fraction of constituent fibres was also an important feature in determining the strength of materials [16].

In order to gain insight into specific features of deformation and damage of the fibrous

network, a micromechanical numerical model was developed. Various numerical approaches are used in literature to simulate the mechanical behaviour of fibrous materials [6, 14, 20, 22, 23]. These approaches can be basically divided into two main categories - continuous and discontinuous (i.e. discrete) - modelling schemes. In discrete methods, the main purpose is to elucidate the effect of microstructure of the material incorporating some specific features such as randomly oriented fibres, pores, bonding points into a computational model; this provides a better understanding of underpinning processes under variety of loading conditions. Therefore, a discrete modelling technique accounting for realistic material microstructure is used in this study. It is a modification of a parametric scheme developed by the authors [22, 25]. A special python script, developed in this research, is used to trim fibres of the fibrous network to introduce notches of various shapes and to discretise models for FE simulations. Deformation and damage mechanisms of a fibrous material are investigated using this numerical model; quantitative assessments of failed fibres, strain distributions in local regions are conducted.

2. Experimentation

2.1. Material

The fibrous material in the core of this research is a thermally bonded calendered 30 g/m^2 nonwoven composed of mono-component polypropylene fibres. A resultant microstructure of the material is sensitive to physical factors such as temperature and pressure in the manufacturing process; it significantly affects performance of the material at macro level. The manufacturing process also defines mechanical behaviour of bond points [26]. To manufacture this thermally bonded nonwoven, the polypropylene fibres are extruded and then stretched to increase their crystallinity [27]. At this stage continuously spun fibres are laid randomly down on a moving conveyed belt, defining non-uniformity of fibre distribution. In the subsequent stage, fibres are bonded by simultaneous application of heat and pressure in a calendering process. Microstructural analysis presents significant differences between bonded and unbonded regions in Fig. 1; the bond points with their spatial pattern and bridging fibres can be easily distinguished. Results of mechanical analysis of single fibres extracted from this material that demonstrate their visco-elasticity and plasticity can be found elsewhere [28].

2.2. Experimental Procedure

The characterization of a fibrous material and understanding of its deformation and damage mechanisms require experiments on fabric as well as on its constituent fibres. Single-fibre tests are essential for implementation of discrete FE simulations as fibres are the basic component of the fabric and play an important role in defining its overall mechanical behaviour. Therefore, single fibres were tested under tensile loading conditions to quantify their material properties. Together with this, fabric tests were performed to investigate notch sensitivity of its deformation and damage behaviours. The tensile tests for various notches were performed and respective force extension diagrams were recorded. A number of images was taken during the stretching process of specimens to assess the damage evolution and factors causing the ultimate failure of the material.

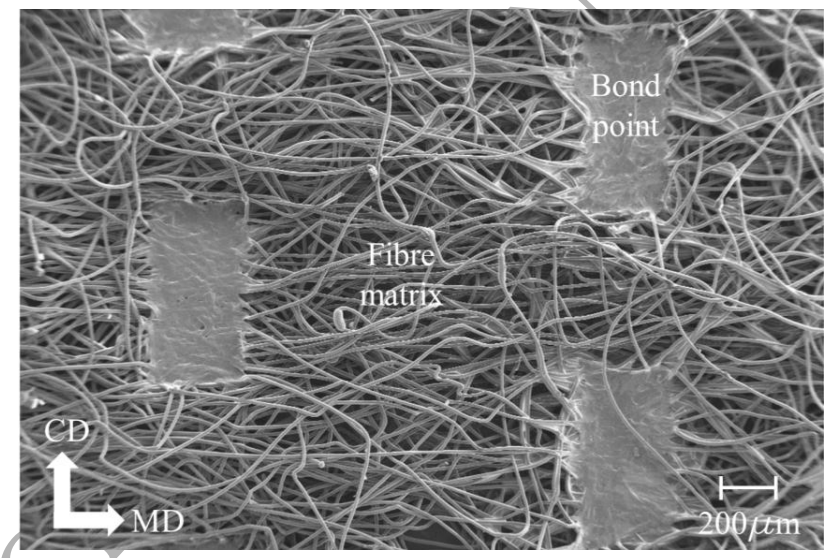

Figure 1: SEM image of 30 g/m^2 thermally bonded calendered nonwoven

2.3. Single-fibre Tests

The material properties of single fibres (with a circular cross-section and a diameter of 18 μm) extracted from the studied thermally bonded fabric are different from those of the virgin fibres due to pressure and temperature involved in the bonding process. Hence, individual

fibres extracted from the fabric were used to obtain their material properties. The tensile tests were carried out at various levels of constant engineering strain rates - 0.5, 0.1 and 0.01 s^{-1} - using Instron Micro Tester 5848 with a high-precision 5 N load cell; full details of the experimentation are given in [22]. The elastic-plastic properties obtained from the single-fibre tensile tests were used as input into the finite-element model of the fibrous network. The respective nonlinear relationships between true stress and plastic strain are given in [22]; the elastic modulus and the Poisson's ratio of fibres were obtained as 350 MPa and 0.42 [22]. A (relatively low) strain-rate sensitivity of fibres was not considered. It was assumed that bond points had the same elastic-plastic properties as the fibres.

2.4. Fabric Tests

Samples of the fabric were prepared in form of rectangular and square coupons with the dimensions of 25 x 25 mm^2, 50 x 50 mm^2, 25 x 50 mm^2 and 50 x 100 mm^2. Four types of central notches - a circular hole, a single vertical cut, a square and a diamond holes - were produced in the centre of the samples using a surgery knife to obtain precisely defined geometries.

These types represent most common cases of defects observed in real life. Various sizes of nonwoven coupons helped to understand the effect of a specimen size and shape on deformation and damage mechanisms alongside analysis of notch sensitivity. The initial dimensions of samples and central notches are presented in Table 1 and specimens with four different notches are shown in Fig. 2.

Table 1: Dimensions (in mm) of samples w x l (width x length) and notches D (in mm) (see Fig. 2)

Samples	25 x 25	50 x 50	25 x 50	50 x 100
Circular hole, diameter	6.35	12.7	6.35	12.7
Square hole, side	6.35	12.7	6.35	12.7
Vertical cut, length	6.35	12.7	6.35	12.7
Diamond hole, diagonal	6.35	12.7	6.35	12.7

In addition to these notched samples, non-damaged samples with the same four sets of dimensions were produced as reference points for comparison. The samples with notched and virgin configurations were cut out along MD. The fibrous samples were tested with a Hounsfield testing machine in MD and CD with a strain rate of 0.2 s^{-1} employing a load cell of 100 N, according to ASTM D4595 (2011). The tests were repeated 5 times for each type of specimens.

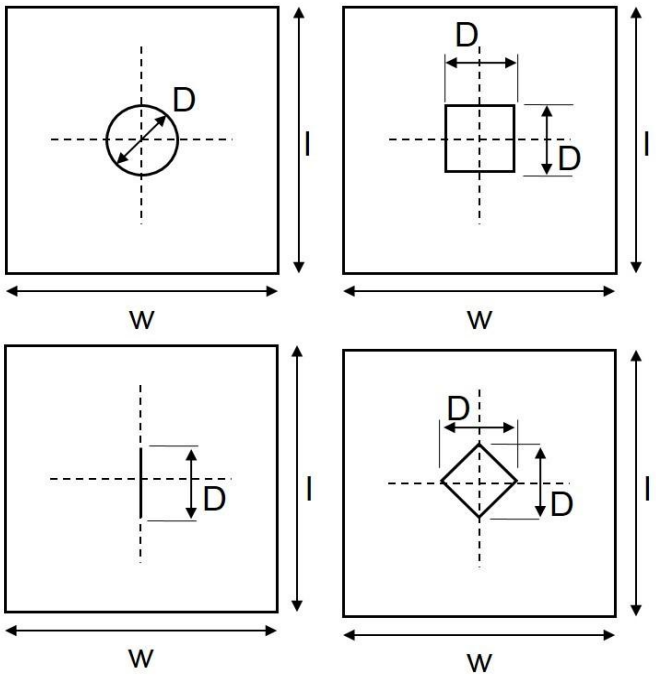

Figure 2: Dimensions of specimens with four different central notch shapes (loading direction is vertical)

2.5. Geometric Properties of Fibrous Network and Fibre Orientation Distribution Function

Characterisation of microstructural features of the undeformed fibrous network (fabric) was performed using scanning electron microscopy (SEM); one of the typical images obtained with SEM is shown in Fig. 1. Dimensions of structural entities such as bond points and their pattern as well as orientation distribution of fibres were required to develop the finite-element model from these images. The orientation distribution function (ODF) of fibres was determined by using in-house software detailed in [5]. The dimensions of bond points and other geometrical elements required to model the network are given in Fig. 3 and Table 1.

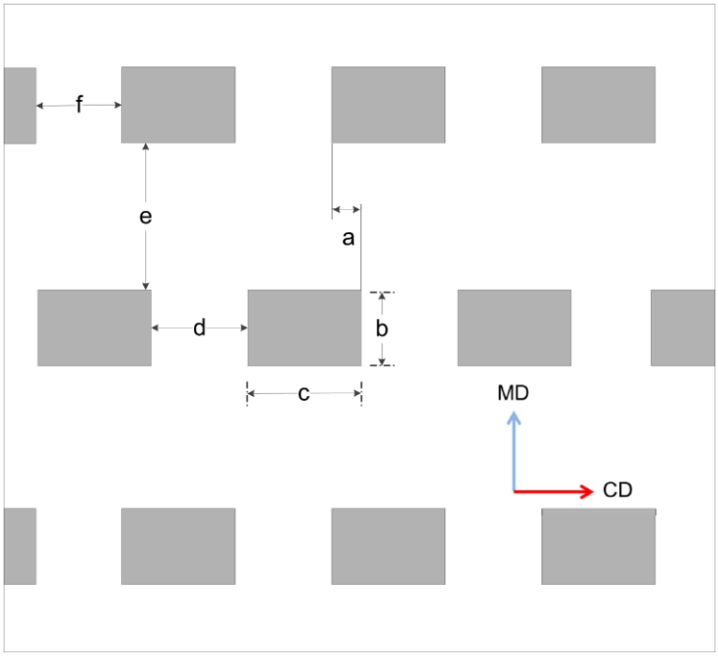

Figure 3: Bond pattern of nonwoven with its dimensions measured from SEM images (a = 0.06 mm; b = 0.47 mm; c = 0.84 mm; d = 0.74 mm; e = 1.60 mm; f = 0.79 mm; average based on 5 measurements)

3. Discontinuous Finite-element Modelling of Fibrous Network

A 3D finite-element (FE) model of the fibrous material incorporating realistic materials microstructure was built using a specially developed parametric code [25]. FE models of various fibrous materials generated by this code explained complex deformation and progressive failure mechanisms successfully in our previous studies [22, 25]. Evaluation of orientation of fibres and positions of bond points in fabrics exposed to stretching in two main orthogonal directions (MD and CD) were simulated and validated by experiments [25, 29]. Using the same code, samples with circular and square notches as well as vertical slits were generated and discretized in commercial FE software, MSC Marc-Mentat. All the notches were placed in the centre of the specimen using their x-y coordinates; the same pattern of bond points was employed in all the models (see Fig. 10). To generate a fibrous network, at first stage, continuous fibres were randomly distributed and oriented based on the measured

orientation distribution function in the same plane, obtained from SEM images of the specimens. Notches were introduced automatically by a python code outlining fibres using quad surfaces after the generation of initial geometry without notches. A flow chart of the algorithm used to generate the discretized finite-element model for notched specimens is presented in Fig. 4.

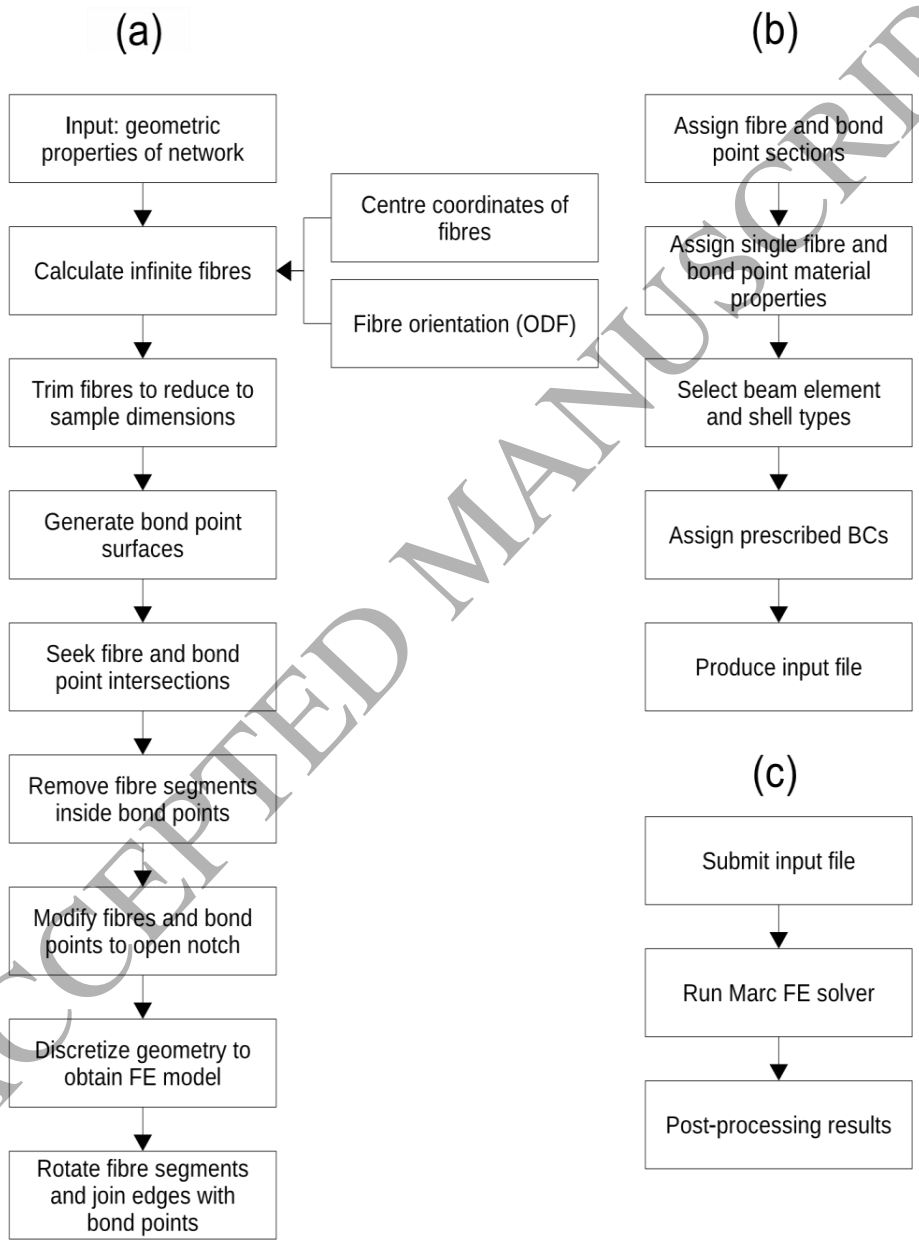

Figure 4: Flow charts of fibrous-network generation algorithm (a), pre-processing (b) and solution with post-processing (c)

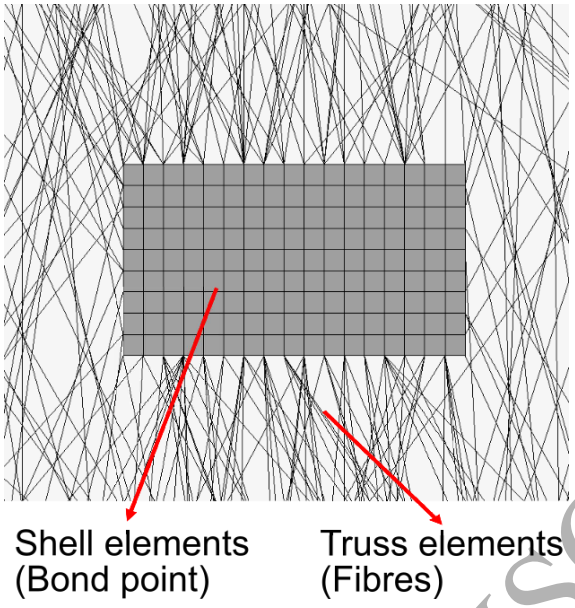

Figure 5: Zoomed view of bond point and fibres in FE model

In MSC Marc [30], two-node truss elements (element id 9) for fibres and thin-shell elements (element id 139) for bond points were selected with thickness equal to that of the points in the modelled fabric. Weak formulation for a momentum equation for a truss-shell system is given by

$$\delta W_{int} = \delta W_{ext} \tag{1}$$

where δW_{int} and δW_{ext} are internal and external virtual works, respectively. Internal virtual work for a truss in absence of transverse shear and moments is

$$\delta W_{int}^{truss} = \int_0^L (N_z \delta \varepsilon_z)\, dz, \tag{2}$$

i.e. the work done by axial force N_z. In a local coordinate system, z-axis coincides with the longitudinal axis. For the bond points, thin-shell elements were selected due to their relatively low thickness compared to their length and width; each bond point was discretized by 153 thin-shell elements (as seen in Fig. 5). The bond points and fibres were represented one-to-

one in FE models. So, 29916 shell elements and 19770 truss elements were employed in the case of the virgin specimen (the numbers were somewhat smaller in other models depending on the type of the notch). Importantly, all mechanical properties as well as initial geometric parameters of the fibrous network and a pattern of bond points (before introduction of the notches) were the same, allowing direct comparability of the developed models.

An internal virtual work for a shell element based on a Discrete Kirchhoff Theory in absence of shear deformation in x and y (in-plane) is given by

$$\delta W_{int}^{shell} = \int_0^L \left(M_x \delta\kappa_z + 2M_{xy}\delta\kappa_{xy} + M_y\delta\kappa_y\right) dA, \tag{3}$$

This is the sum of virtual works done by the bending moments M_x and M_y, and the twisting moment M_{xy}. κ_y, κ_z and κ_{xy} are curvatures. The total virtual work was computed from contributions of truss and shell elements:

$$\delta W_{int} = \sum_{i=1}^{n} \delta W_{int}^{truss} + \sum_{i=1}^{m} \delta W_{int}^{shell} \tag{4}$$

Material behaviour of single fibres was incorporated in the incremental form of elastic-plastic stress-strain relations [30, 31] using a basic assumption that the deformation can be divided into its elastic and plastic parts. The general form of this for the total deformation gradient is [30]

$$F = F^e \cdot F^p, \tag{5}$$

where indices e and p denote the elastic (reversible) and plastic parts, respectively. The finite-element software usually employs an additive strain-rate decomposition [30]

$$\dot{\varepsilon} = \dot{\varepsilon}^e + \dot{\varepsilon}^p, \tag{6}$$

where ε^e and ε^p are elastic and plastic strain tensors. Then, the Cauchy stress can be expressed as

$$\dot{\sigma} = C : \dot{\varepsilon}^e = \dot{\varepsilon} - \dot{\varepsilon}^p. \quad (7)$$

The slope of a hardening curve (i.e. work-hardening coefficient) H is given as

$$H = d\sigma_{eq}/d\varepsilon_{eq}^p\,, \quad (8)$$

where σ_{eq} and ε_{eq}^p are equivalent stress and equivalent plastic strain, respectively. The flow rule in work hardening has the form:

$$d\varepsilon^p = d\varepsilon_{eq}^p : \nabla\sigma_{eq}, \quad (9)$$

and the equivalent plastic strain increment is

$$d\varepsilon_{eq}^p = \frac{\nabla\sigma_{eq} : C : d\varepsilon}{H + \nabla\sigma_{eq} : C : \nabla\sigma_{eq}}. \quad (10)$$

The slope H was computed from the experimental curves. It should be mentioned that fibre curvatures and fibre-to-fibre interactions were neglected in this research. Our previous works demonstrated that the curvature and friction do not make any significant contribution to deformation and damage mechanisms in uniaxial tensile tests of such materials [22, 32]. However, the curvature might increase the material's toughness by increasing the maximum strain in a stress-strain response. The simulations of tensile tests were carried out by applying a set of boundary conditions to the FE model, within the framework of the implicit algorithm for quasi-static loading with large displacements. The nodes on one side of the generated model were fully constrained to reflect the fixing conditions of pneumatic grips used in the tensile experiments whereas a uniform axial displacement with a changing magnitude corresponding to the strain rate of 0.2 s^{-1} was applied to the nodes on the opposite side of the model.

4. Results and Discussion

4.1. Tensile Performance of Fibrous Networks

The ODF of the selected fibrous medium, which was obtained using inhouse software, is presented as a histogram in Fig. 6; it shows preferential orientation of fibres in MD (90°) and, thus, quantifies the extent of anisotropy of the fibrous network. The normalized force-extension curves of the specimens in MD for both virgin and notched specimens are shown in Fig. 7. After five tensile tests along MD for each configuration, the median load-displacement curves were selected for analysis since the results demonstrated a significant scatter after the onset of damage (the initial stages of loading were similar for each case). The forces were normalised by using an effective width (the difference between the specimen width and the notch width) that varied depending on dimensions of the sample and the notch. The following conclusions can be made based on the experimental observations:

- Deformation behaviour of fibrous specimens in MD direction had a different level of sensitivity to various shapes and aspect ratios of the introduced notches.
- The levels of tensile strength of virgin specimens and specimens with a vertical slit were nearly the same. The main reason for this result is that the alignment of most fibres was in MD, and their contribution to the load-carrying capacity was not affected significantly by a vertical cut.
- The samples with circular notches showed lower toughness. This behaviour agrees with the findings in [16].
- Ultimate strength was not influenced by the aspect ratio and the size of specimens. Conversely, the statistical analysis of experimental data for maximum extension demonstrated that it was influenced significantly by the aspect ratio.

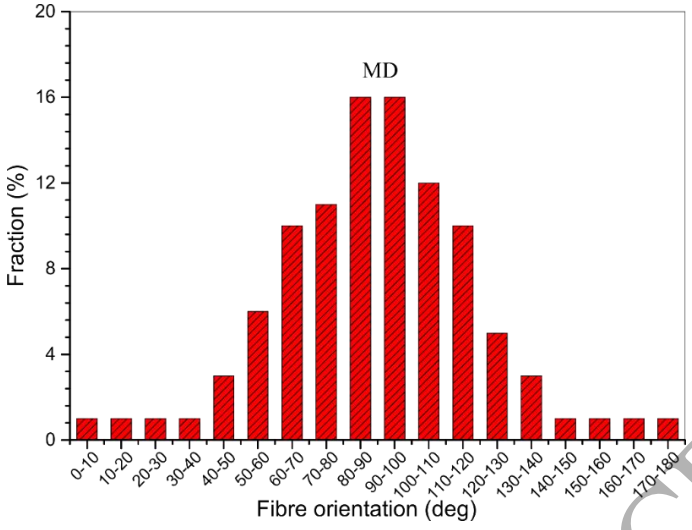

Figure 6: Orientation distribution of fibres calculated from SEM images of selected 30 g/m^2 nonwoven (MD corresponds to 90°).

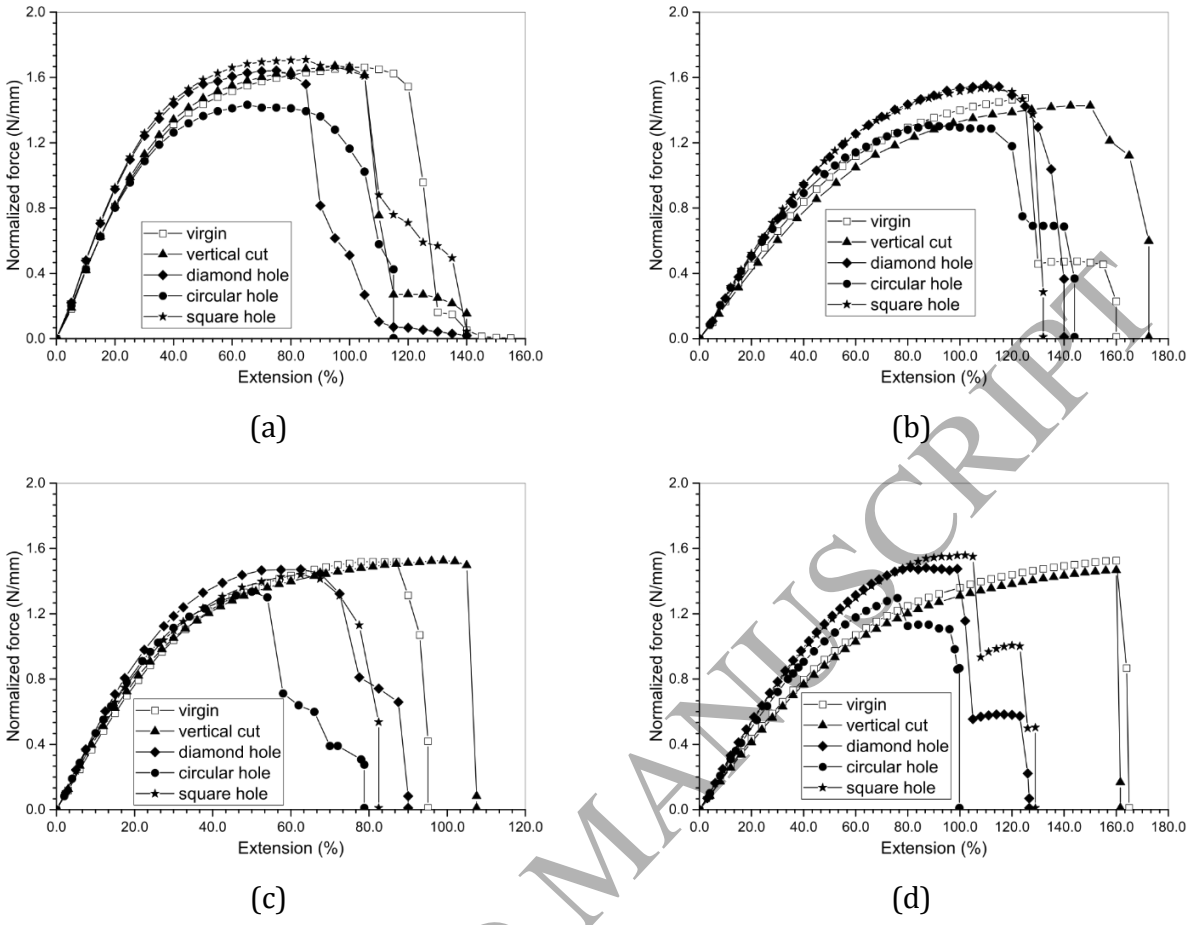

Figure 7: Experimental mean force-extension curves of virgin and damaged samples in machine direction for specimens of different dimensions: (a) 25 mm x 25 mm; (b) 25 mm x 50 mm; (c) 50 mm x 50 mm; (d) 50 mm x 100 mm (averaging over 5 specimens)

In Figure 8, the damage evolution in virgin specimens and specimens with four types of used notches is presented. From the perspective of the microscopic structure, in the tensile test, before fibres start participating in a load transfer, they are straightened from their initial curved form. At the same time, fibres start realigning themselves towards the loading direction. At the early stage of the axial deformation, apparently, notches in the samples grew in both MD and CD. The damage growth in CD slowed down before failure of fibres, while the growth in MD continued. In samples stretched along MD, weak areas (with lower spatial density of fibres) occurred at arbitrary locations. Further deformation led to the growth of some of these areas with an increase in failed fibres, which are the source of damage localization in the matrix. For the virgin specimens of various dimensions, the potential

regions of damage localizations were hard to predict, while, in specimens with square, diamond and circular notches, the localization of damage zones was near notches as anticipated. Sharp edges of the notches became blunted as a result of this process. This is mainly associated with re-orientation of fibres towards the loading direction, i.e. toughening of the fibrous network. Fibres around the circular notch were deformed considerably as observed by comparing changes in distances between bond points, aligned in a regular pattern before application of a tensile load. Axial distances between the neighbouring bond points were the same at initial state and, by extending the specimen, these distances increased around the circular notches during the tests. For instance, under 60% extension, the axial distance between two adjacent rows of bond points near the edge of the notch and close to its horizontal axis of symmetry increased by the factor of 3.03, while it grew by 93% at the level of the axial head of the deformed notch (Fig. 8c).

A non-uniform (and, hence, non-symmetric) distribution of individual fibres in the matrix triggered rotation of bond points by different amounts depending on their location and loading direction. Their behaviour is more unpredictable due to complex interaction between bond points and attached fibres. With some fibres in the matrix cut, the load that they carried was transferred to other fibres via random sets of links between bond points and fibres. Such a discontinuous load-transfer mechanism resulted in diffused local loads, instead of concentrating it in the vicinity of the notch or even causing stress singularity as in traditional continuous materials.

Table 2: Ratio of damage area measured at maximum stress (A_{max}) to initial damage area determined at initial strain (A_0) for loading in MD direction.

	Diamond hole	Circular hole	Square hole	Vertical cut*
*Amax/A*0	4.8	7.4	4.6	3.1

*For the vertical cut, the level of damage is defined as the change in the slit's length.

Employing digital image processing software, damage areas (occupied by a notch) of the tested specimens at its initial state A_0 and at the maximum force A_{max} were measured; the ratio between the latter and the former was calculated. These ratios are given in Table 2 for

different notches. For stretching in MD, this ratio for the circular notch is clearly higher than that for other specimens. From normalized force-extension diagrams in Fig. 7 it is obvious that specimens with circular holes started failing much earlier than their counterparts.

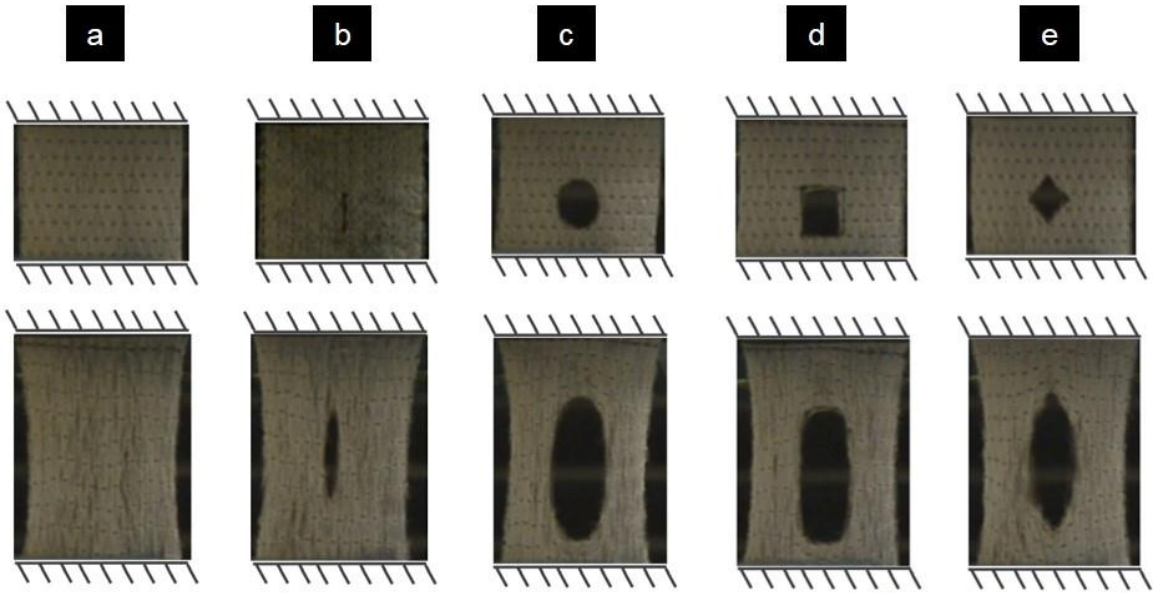

Figure 8: Damage evolution in 25 x 25 mm^2 polypropylene fibre samples under 60% extension in MD: (a) virgin; (b) vertical cut; (c) circular hole; (d) square hole; (e) diamond hole

From the same figure, it is clear that maximum levels of strength of the samples were almost the same for various sample dimensions as they were normalized by the sample width. Therefore, the effect of sample size on tensile performance of the fibre network was insignificant. As for the virgin samples, their damage and failure mechanisms were investigated in [22]. Upon reaching failure strain, first fibres failed, and this initiated damage in fibrous networks. Randomly oriented fibres in the network failed progressively resulting in a gradual growth in damage observed. Topological changes due to the damage initiation and growth were also simulated in the same resource; major changes in fibre orientation distribution were calculated.

4.2. Finite-element Simulations

Tensile and damage behaviours of virgin, vertical-slit, square and circular notches were successfully simulated with the developed model. A maximum strain damage criterion for

fibres was incorporated into the models, with specimens stretched till their complete failure. The damage parameter D and the failure criteria are expressed in following form:

$$\text{if } D = \left(\frac{\varepsilon_z}{\varepsilon_f}\right) \geq 1.0, \text{ fibre fails.} \qquad (11)$$

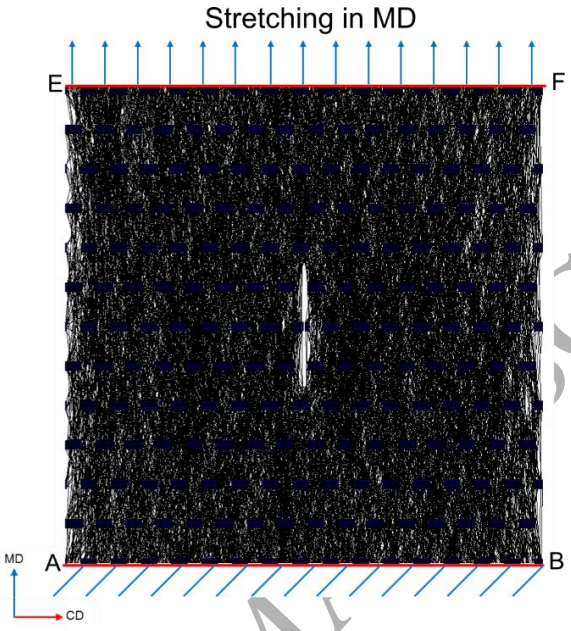

Figure 9: Boundary conditions

In simulations, fibres were assumed to exhibit a fully isotropic material response, and the failure strain ε_f was taken 1.0 from single-fibre tests. As a strain along the longitudinal axis in each truss element representing a fibre segment in the FE models exceeded the failure strain, it considered as failed and was deleted. Boundary conditions applied to the specimen with a vertical cut are given in Fig. 9 for two segments AB and EF. In simulations, the nodes on AB were fixed in two main directions - MD and CD, while nodes on EF were fixed in CD only and the FE model was stretched in MD by displacing edge EF. The nodes at both boundaries were allowed to rotate. Images of the virgin, slit-, square- and circular-notched specimens obtained in tests at 0, 60, 80 and 100% of fabric's axial extension are shown in Fig. 10 in comparison with experimental observations. Apparently, the models are capable to reproduce main deformation and damage features including a necking effect linked to fixture of specimens in the grips observed in the performed tests.

Additionally, the variation in notch geometry caused by the deformation of the fabric was well captured; blunting of sharp edges of the notches in experimental samples was reproduced in FE simulations. The square notch in both simulations and experiments was changed into a rectangle-like damage area with blunted corners. The vertical-slit notch became an elliptical hole with a very low width-to-length ratio. The circular notch caused an elliptical hole with a higher aspect ratio than the vertical notch. In addition to the damage evolution around the notches of the samples, a similar re-alignment of bond points occurred in both experiments and simulations. Fig. 11 demonstrates alignments of bond points in virgin, slit-, square- and circular-notched specimens for various extensions. Re-alignments of bond points in virgin specimen exhibited similar behaviour with slit-notched specimen by 30% extension. Deformation in both specimens were concentrated in different locations by higher extensions (60% and 100%), and damage propagated in different paths. Alignments of bond points around the square and circular notches showed different behaviour than in the case of the slit notch at 30% extension. At higher extensions (60% and 100%), distances between bond points increased and the cracks (damage zones) became more visible. These zones exhibited nearly the same inclination with regard to the stretching direction. Still, further studies were essential to reveal micromechanisms of failure, which are presented in the next section.

4.3. Failure Model and Failure Analysis

The detailed deformation, damage and failure mechanisms of fibrous networks are examined in this paper to provide basic understanding of growth of damage, localization of deformation and failure evolution.

Localized damage evolution is still not understood as it is cumbersome to follow the mechanisms at microscale due to limitations of in-situ visualisation techniques. Only relatively small samples might be tested in-situ with SEM, because the space in SEM visualisation chamber is limited. Thus, the selected sample size can cover only a few bond points and not many fibres. Besides, in formation of fibre bundles around those bond points, the edge effects should not be neglected. So, FE simulations provide an alternative way to measure and observe microscopic changes in fibrous networks. It is apparent that fibres in the network were introduced according to the measured ODF at the initial stage with a significant level of

disorder. Under axial stretching, the notch opened with increasing tensile loading and fibres reoriented themselves towards the loading direction. As a result of this spatially non-uniform process, the most loaded fibres (oriented predominantly at small angles to the loading direction) started failing, causing load redistribution to other fibres in their vicinity. This triggered localisation of deformation and fibre failures in regions, randomly distributed in the simulated fibrous networks, as obvious from the numerical results for large extensions (Fig. 10). These processes are more apparent when evolution of bond-point patterns is considered (Fig. 11): the initial axial and lateral distances between bond points were equal; at high deformations, they changed, in many cases significantly.

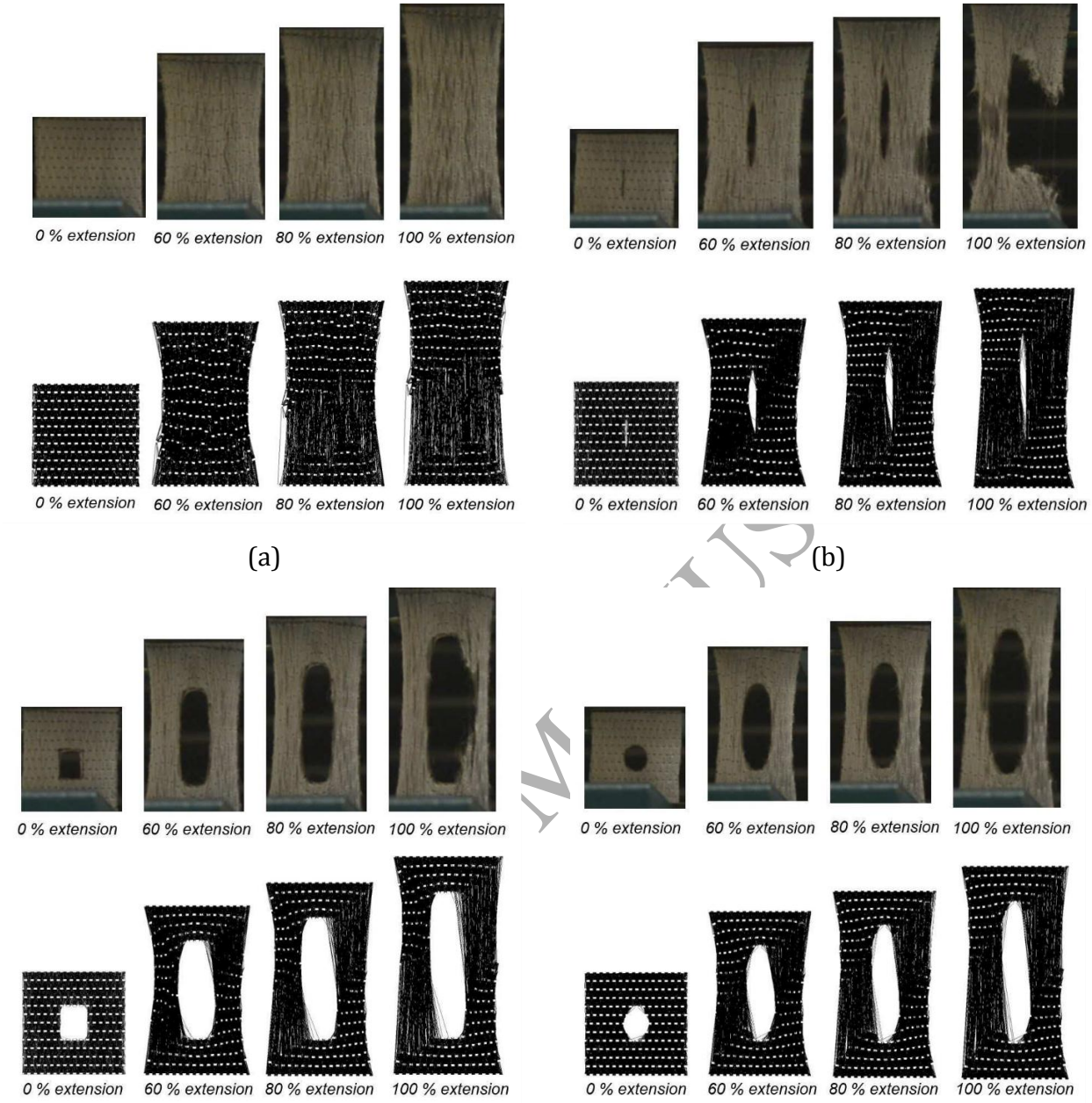

Figure 10: Comparison of experimental and simulated damage patterns for virgin (a), slit-notch (b), square-notch (c), circular-notch (d) specimens for 0%, 60%, 80%, 100% extension.

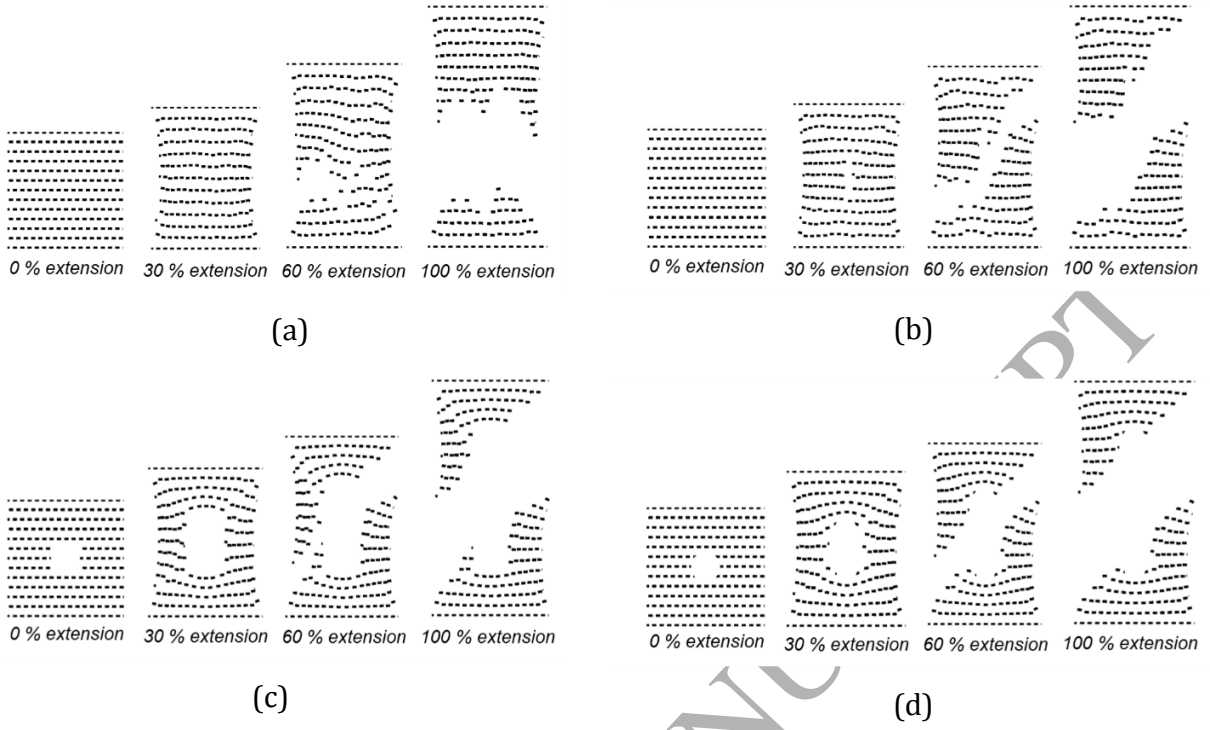

Figure 11: Alignment of bond points for 0%, 30%, 60%, 100% extension of different specimens: (a) virgin, (b) slit notch, (c) square notch, (d) circular notch

The developed model can be used to analyse the microstructural changes at any level of extensions. A histogram of normalised fibre strains is demonstrated in Fig.12 for virgin specimens at 40%, 60%, 80%, and 100% extensions; logarithmic strains were normalised by failure strain of fibres, hence demonstrating their closeness to rupture. Most of normalised strains were in the range between 0-0.5 in 40% extension, and far below the level required for failure. As the FE model was stretched further, more fibres exceeded the value of 0.5. The normalised strain distribution in 80% extension fell back below 0.5. As the extension value increased from 60% to 80%, 5% of constituent fibres in the virgin specimen failed. These failed fibres altered the network's microstructure and, therefore, some of fibres in MD shifted back to their original positions. As the network was stretched, fibres re-aligned themselves towards the loading direction (MD). A similar behaviour was observed in [33] employing SEM.

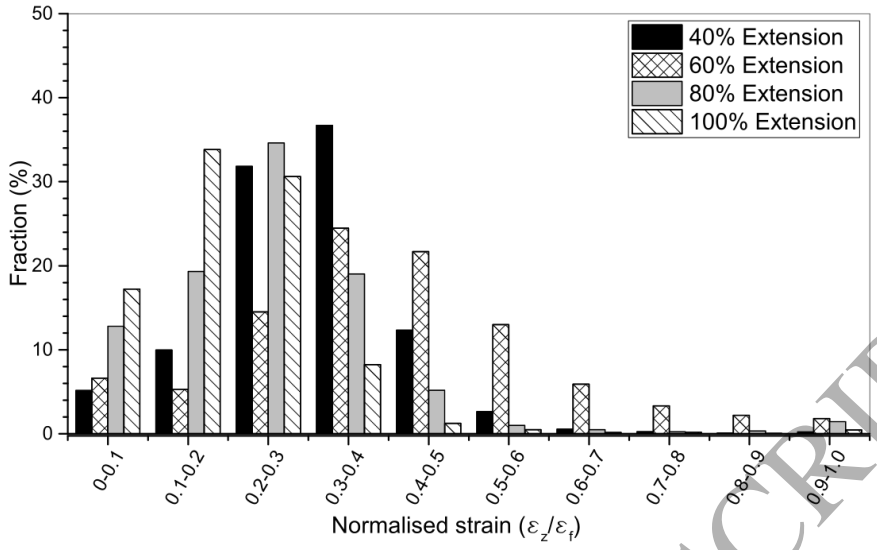

Figure 12: FE-based calculated distributions of fibre strains (normalised by failure strain of fibres) in virgin specimen for fabric extension of 40%, 60%, 80%, and 100%.

Another way to assess the data for fibre strains is to compare them with the global deformation (stretching) of the fabric. Such histograms are presented in Fig. 13 for un-notched specimen, with fibre strains normalised by that of the fabric specimen. Generally, only a rather small fraction of fibres exhibited levels of strains in excess of that of the fabric; most had strains smaller by a factor of more than 2. Interestingly, that at higher extensions (more than 60%), the median of distribution moved towards the lower strains with the growing global deformation, meaning that an increasingly small number of fibres carried the external load. Quantification of this change in fibre-orientation distribution is given in Fig. 14 for various level of extensions. At higher extensions (80% and 100%), more of the fibres were counted in the range of 0-10 degree than in 40% extension. This is pertaining to the fibres relaxed due to failure, and, therefore, the contraction behaviour is more visible in this figure.

As for notched specimens, in the slit-notch case, higher strain localisations were triggered around the sides of the samples; this behaviour can be seen in Fig. 10 (b). The slit could not constrain higher strain, and a failure zone formed around the induced damage. Different deformation behaviour was caused by a square notch: tracking of distances between bond points showed their nearly symmetrical distribution over the sample before the onset of failure of individual fibres. Strain was much more localised around the induced damage. First

fibres started failing as the overall extension of 58%, and they occurred near the induced damage tip as shown in Fig. 15. Fibres parallel to the loading direction (MD) in the vicinity of such areas accommodated deformation and increased the resistance to damage propagation in the direction perpendicular to the loading [34]. In the case of fibre-to-fibre bonds in a fibrous network, the tensile strength of the notched specimens might be also improved by fibre bridging [35].

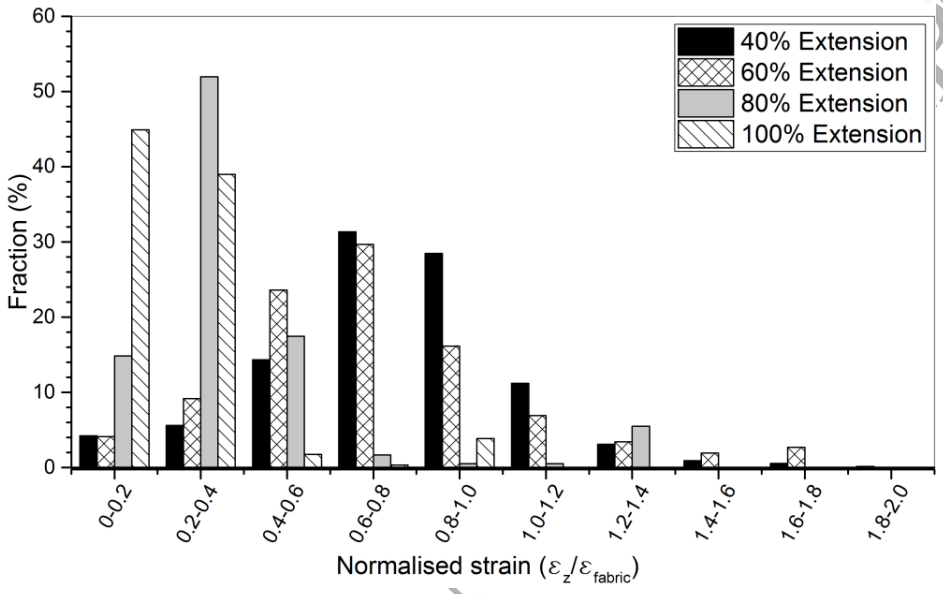

Figure 13: FE-based calculated distributions of fibre strains (normalised by failure strain of fabric) in virgin specimen for fabric extension of 40%, 60%, 80%, and 100%.

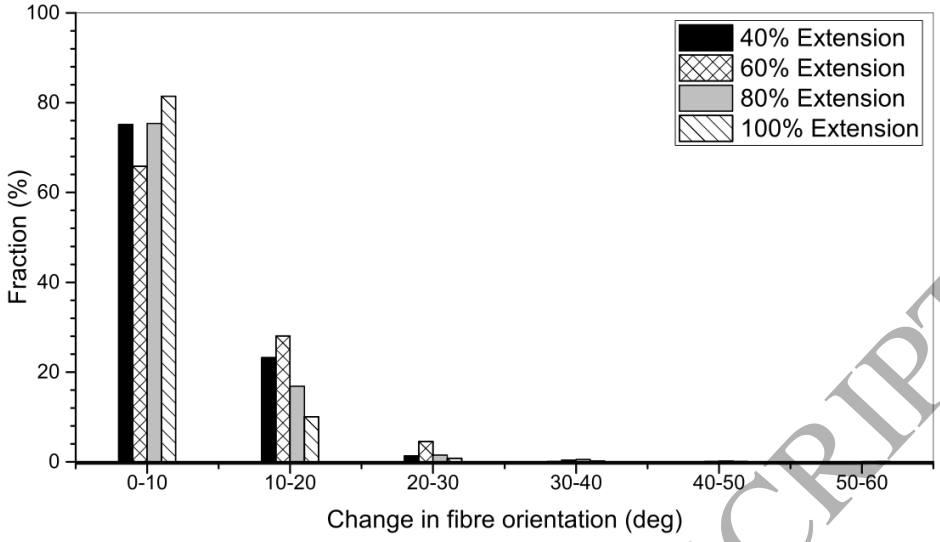

Figure 14: FE-based calculated distributions of change in fibre orientation for virgin specimen for fabric extension of 40%, 60%, 80%, and 100%

The constituting fibres of samples demonstrated ductile behaviour and some of them could be stretched to double lengths. In our studies, fibres between nodes of two parallel paths (path-1 and path-2 in Fig. 16) were tracked to reveal localisations of strain and failure. For the sake of brevity, only slit-, square- and circular-notch samples were analysed in this study. The paths were chosen in the way so that one - path-1 - connected the longitudinal axis and the edge of the specimen along the lateral direction ahead of the notch, while another - path-2 - was parallel to path-1 and started at the notch's edge. In order to get more uniform fibre distributions in the selected intervals of the tracked paths, the paths were selected to avoid bond points. For the slit-notch case, distributions of logarithmic strain over path-1 and path-2 corresponding to various extension levels are presented in Fig. 17. A non-uniform strain distribution over path-1 was obtained in simulations: a sharp increase around the centre of path-1 was apparent. An increase in strain levels over path-2 at the notch tip was observed; however, this did not cause failure of any fibres over the same path (as discussed, the failure strain of individual fibre ε_f = 1.0.). In the case of the square notch (Fig. 18), behaviour close to that of continuous materials such as rubber was observed, with strains rising towards the square notch. As for the circular notched specimen (Fig. 19), apart of a small increase in strain at the notch tip, no sharp increase - as in continuous materials - was found.

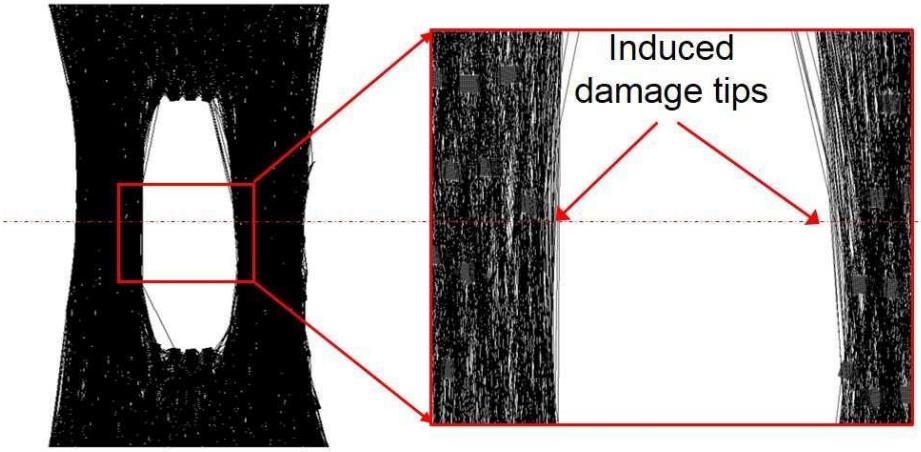

Figure 15: Induced damage tips

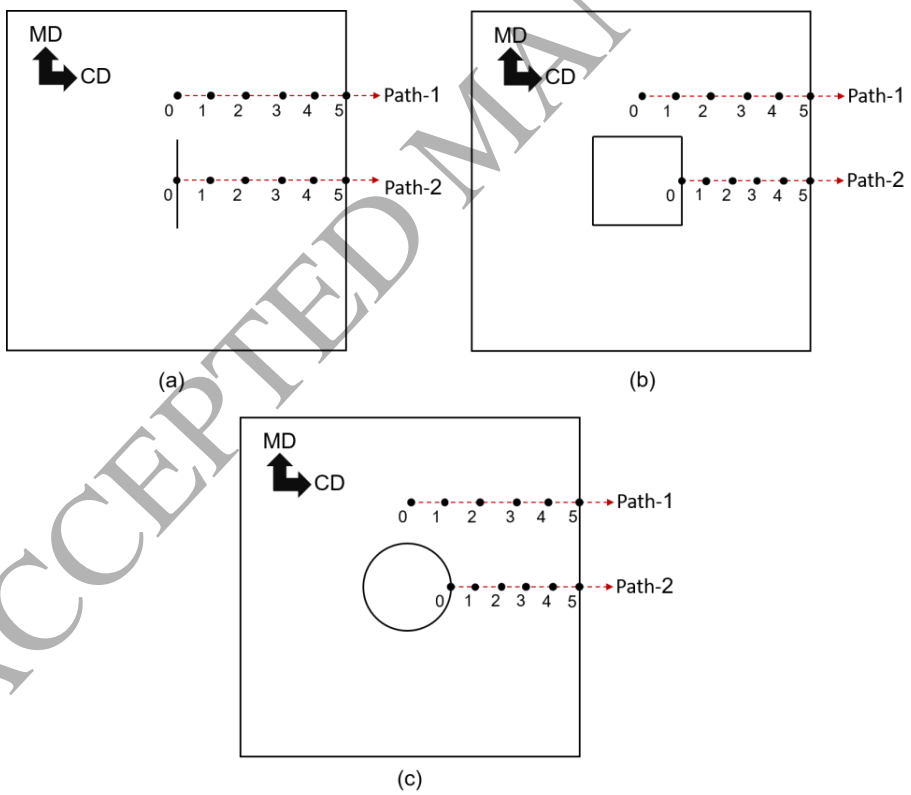

Figure 16: Two paths selected for slit-notch (a), square-notch (b) and circular-notch (c) models

This difference can be explained by distinct load-transfer mechanisms. For instance, in a network, a fibre under high deformation connecting the edges of the notch and the specimen may not transfer this deformation to other fibres in its neighbourhood if it lacks any connection to them. In contrast, continuous materials can easily transfer the load along loading and transverse directions. Furthermore, this small increase also stems from large nonlinear deformation capacity of polymer materials leading to the blunting of the notch tips [36]. It was reported [37] that circular notched specimen resulted in lower tensile performance than virgin samples and specimens with vertical and horizontal slits. This behaviour was attributed to a higher number of cut fibres contributing to the load transfer in comparison to other damage cases.

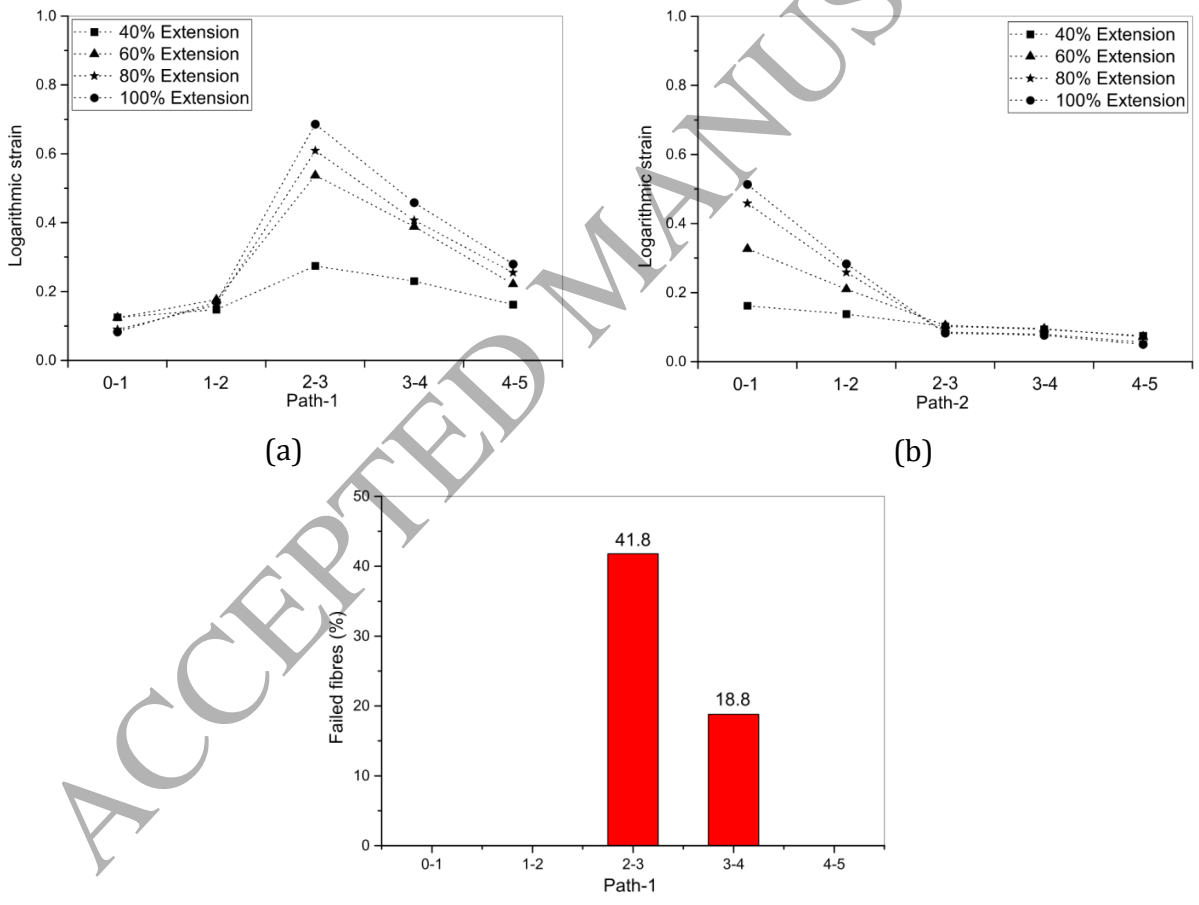

Figure 17: FE-based calculated distributions of fibre strains in case of slit notch over path-1 (a) and path-2 (b) for various levels of extension of specimen; (c) fraction of failed fibres along path-1 at extension of 100%

The FE models with slit, square and circular notches demonstrated different propensities to failure evolution of fibres. Simulations tracked failure of fibres up to 100% extension of the specimens for all these cases in path-1 and path-2. In the slit-notch case, none of fibres failed around the notch (path-2), with fibres failing mostly in path-1. Interestingly, a higher fraction of fibres failed away from the slit axis; none failed in front of it. In same way, edges were more strong initiators of damage than the notch. In the case of the square notch, fibres failed over path-2 and in the middle of path-1. Hence, for path-1, a damage scenario was somewhat similar to that for the same path in the case of the slit. The mechanisms of a decreasing fraction of failed fibres towards the axis was different - a shielding effect of the wide notch. Therefore, a notch in samples can affect stresses in a fibrous network significantly, and the notch shape is another important factor defining strain localization around a notch to trigger failure of fibres. On the other hand, no fibre over path-2 in the case of the circular notch failed as a result of low strains over the same path.

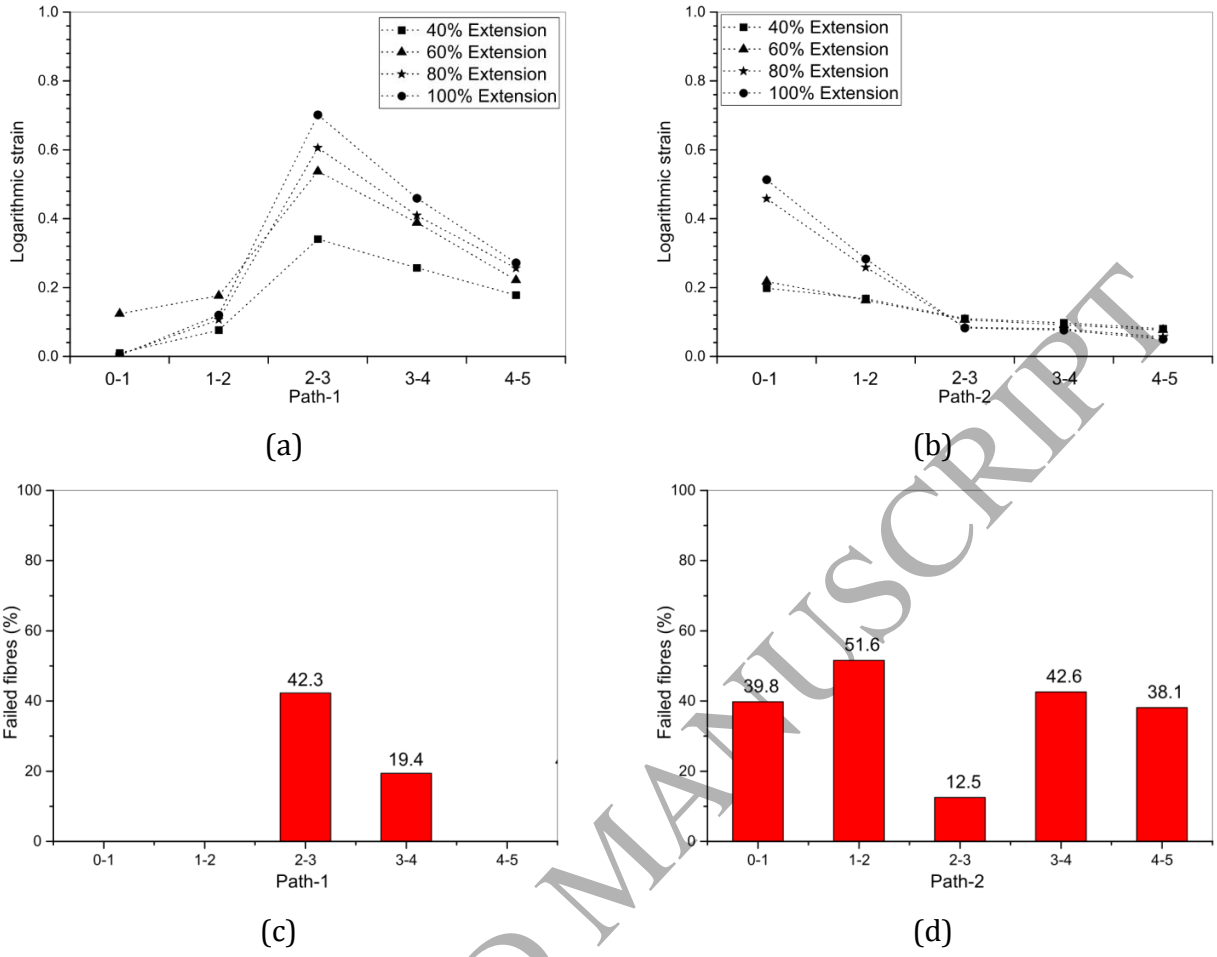

Figure 18: FE-based calculated distributions of fibre strains in case of square notch over path-1 (a) and path-2 (b) for various levels of extension of specimen; fraction of failed fibres along path-1 (c) and path-2 (d) at extension of 100%

5. Conclusions

This paper aimed to understand the micromechanisms of damage evolution in a specific case of a random fibrous network - nonwoven material and to investigate the leading factors controlling damage localizations. Tensile tests were conducted on a group of samples with various notch shapes and various specimen's aspect ratios, along with the samples without any notches. In experiments, it was found that the notch shape had a significant effect on toughness of the fibre network, while the sample size did not affect tensile strength. The samples with the longitudinal notch showed deformation and damage performances similar to those of the samples without a notch. In FE simulations it was demonstrated that such a notch

did not result in any significant increase in localized strain distribution around it. A detailed examination of the fibre networks demonstrated that its initial response was to reorient the fibres towards the loading direction forming their bundles. During this process, the notch opened and damage grew in the loading (MD) and lateral (CD) directions. At the advanced stage of deformation, the damage growth diminished in MD, but continued in CD. Moreover, the circular notch decreased material toughness along with the ultimate strain and maximum extension. A similar conclusion was drawn in [16]; the circular notch was more detrimental in comparison to the cases with the vertical split. A good agreement between experiments and simulations was obtained for damage growth, strain localizations and damage patterns. These findings should support design of engineered fibrous networks with enhanced deformation and damage performance. Furthermore, the microstructure-based numerical model was capable to demonstrate and assess notch sensitivity. It also captured the effect of evolving microstructure of the fibrous network as a function of fabric strain. The utilised model can analyse the effects of notch shape, size and/or the location of the notch on strains and stresses in each fibre of the deformed networks. The parametric character of the developed model makes it a powerful tool for analysis of the effects caused by changes in any mechanical and/or microstructural features, related to specific fibrous network. Future studies will focus on analysis of the effects of fibre-to-fibre interactions, cross-links (for some fibre networks) and fibre curvature, on deformation and damage behaviours of fibrous networks.

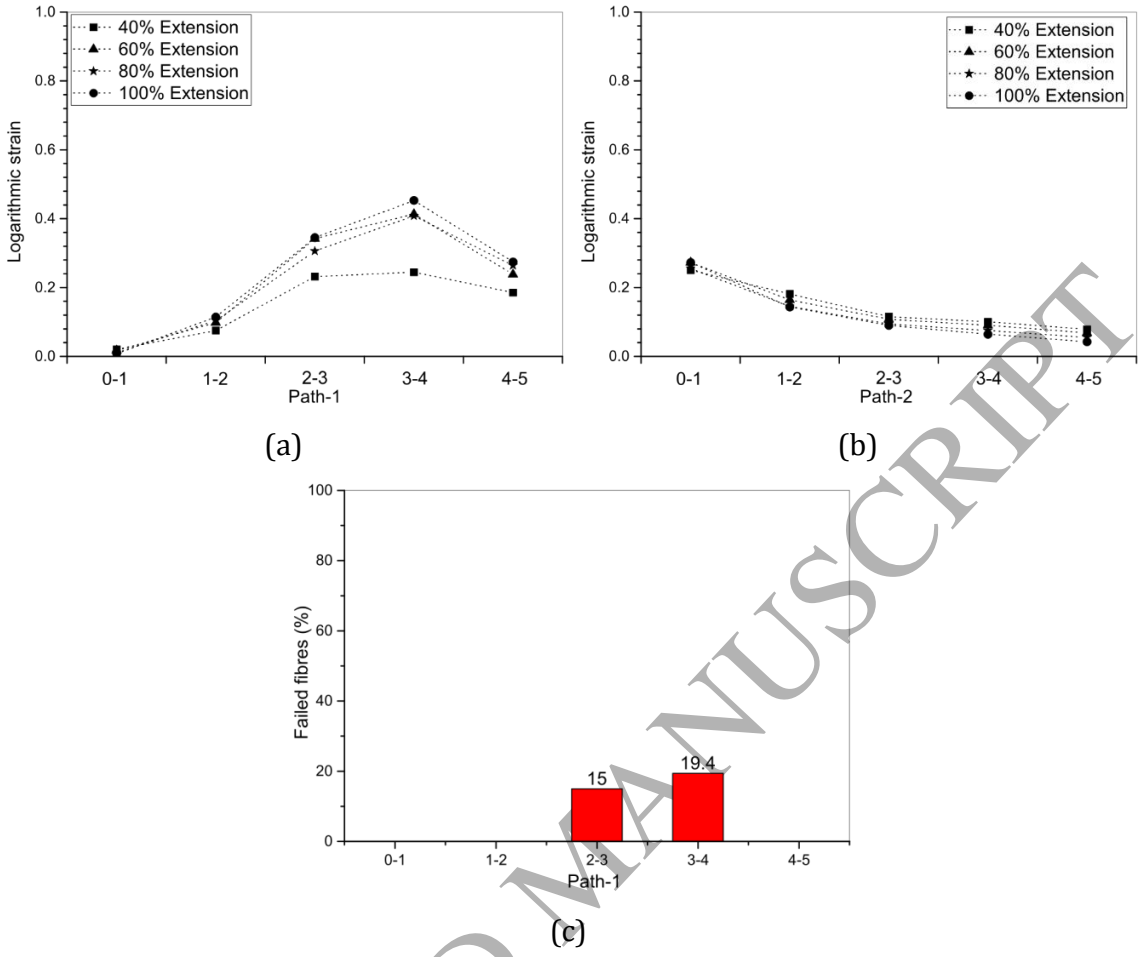

Figure 19: FE-based calculated distributions of fibre strains in case of circular notch over path-1 (a) and path-2 (b) for various levels of extension of specimen; (c) fraction of failed fibres along path-1 at extension of 100%

Acknowledgements

The support by the Nonwovens Institute at North Carolina State University, Raleigh, USA is gratefully acknowledged. The research leading to these results has received partial funding from the European Union Programme Horizon 2020 under Grant Agreement No H2020-MSCA-RISE-2014- 644175 MATRIXASSAY.

References

[1] W. Yang, V. Sherman, B. Gludovatz, E. Schaible, P. Stewart, R. Ritchie, M. Meyers, On the tear resistance of skin, Nature Communications 6 (2015).

[2] K. Jin, Z. Qin, M. J. Buehler, Molecular deformation mechanisms of the wood cell wall material, Journal of the Mechanical Behavior of Biomedical Materials 42 (2015) 198 – 206.

[3] F. G. Torres, S. Commeaux, O. P. Troncoso, Biocompatibility of bacterial cellulose based biomaterials, Journal of Functional Biomaterials 3 (2012) 864–878.

[4] M. Ovaska, Z. Bertalan, A. Miksic, M. Sugni, C. D. Benedetto, C. Ferrario, L. Leggio, L. Guidetti, M. J. Alava, C. A. L. Porta, S. Zapperi, Deformation and fracture of echinoderm collagen networks, Journal of the Mechanical Behavior of Biomedical Materials 65 (2017) 42 – 52.

[5] E. Demirci, M. Acar, B. Pourdeyhimi, V. V. Silberschmidt, Computation of mechanical anisotropy in thermally bonded bicomponent fibre nonwovens, Computational Materials Science 52 (2012) 157 – 163.

[6] E. Demirci, M. Acar, B. Pourdeyhimi, V. V. Silberschmidt, Finite element modelling of thermally bonded bicomponent fibre nonwovens: Tensile behaviour, Computational Materials Science 50 (2011) 1286 – 1291.

[7] F. Farukh, E. Demirci, B. Sabuncuoglu, M. Acar, B. Pourdeyhimi, V. V. Silberschmidt, Mechanical behaviour of nonwovens: Analysis of effect of manufacturing parameters with parametric computational model, Computational Materials Science 94 (2014) 8 – 16.

[8] H. L. Cox, The elasticity and strength of paper and other fibrous materials, British Journal of Applied Physics 3 (1952) 72–79.

[9] E. Ghassemieh, M. Acar, H. Versteeg, Microstructural analysis of nonwoven fabrics using scanning electron microscopy and image processing. Part 1: Development and verification of the methods, Proceedings of the Institution of Mechanical Engineers, Part L: Journal of Materials: Design and Applications 216 (2002) 199–207.

[10] H. Kim, B. Pourdeyhimi, Computational modeling of mechanical performance in thermally point bonded nonwovens, Journal of Textile and Apparel, Technology and Management 1 (2001) 1–7.

[11] D. H. Mueller, M. Kochmann, Numerical modeling of thermobonded nonwovens, International Nonwovens Journal (2004) 56–62.

[12] P. Isaksson, R. H¨agglund, Strain energy distribution in a crack-tip region in random fiber networks, International Journal of Fracture 156 (2009) 1–9.

[13] A. Ridruejo, C. Gonzlez, J. LLorca, Damage micromechanisms and notch sensitivity of glass-fiber non-woven felts: An experimental and numerical study, Journal of the Mechanics and Physics of Solids 58 (2010) 1628 – 1645.

[14] J. Liu, Z. Chen, K. Li, A 2-d lattice model for simulating the failure of paper, Theoretical and Applied Fracture Mechanics 54 (2010) 1 – 10.

[15] L. Beex, R. Peerlings, M. Geers, A multiscale quasi-continuum method for dissipative lattice models and discrete networks, Journal of the Mechanics and Physics of Solids 64 (2014) 154 – 169.

[16] A. Rawal, S. K. Patel, V. Kumar, H. Saraswat, M. A. Sayeed, Damage analysis and notch sensitivity of hybrid needle punched nonwoven materials, Textile Research Journal 83 (2013) 1103–1112.

[17] Y. Chen, A. Ridruejo, C. Gonzlez, J. Llorca, T. Siegmund, Notch effect in failure of fiberglass non-woven materials, International Journal of Solids and Structures 96 (2016) 254 – 264.

[18] X. Gao, E. Sozumert, Z. Shi, G. Yang, V. V. Silberschmidt, Assessing stiffness of nanofibres in bacterial cellulose hydrogels: Numerical experimental framework, Materials Science and Engineering: C 77 (2017) 9 – 18.

[19] C. Peyrega, D. Jeulin, C. Delise, J. Malvestio, 3d morphological modelling of a random fibrous network, Image Analysis and Stereology 28 (2011) 129–141.

[20] J. Dirrenberger, S. Forest, D. Jeulin, Towards gigantic rve sizes for 3d stochastic fibrous networks, International Journal of Solids and Structures 51 (2014) 359 – 376.

[21] A. Ridruejo, C. Gonzlez, J. LLorca, Micromechanisms of deformation and fracture of polypropylene nonwoven fabrics, International Journal of Solids and Structures 48 (2011) 153 – 162.

[22] F. Farukh, E. Demirci, B. Sabuncuoglu, M. Acar, B. Pourdeyhimi, V. V. Silberschmidt, Numerical analysis of progressive damage in nonwoven fibrous networks under tension, International Journal of Solids and Structures 51 (2014) 1670 – 1685.

[23] A. Kulachenko, T. Uesaka, Direct simulations of fiber network deformation and failure, Mechanics of Materials 51 (2012) 1 – 14.

[24] A. Ridruejo, R. Jubera, C. Gonzlez, J. LLorca, Inverse notch sensitivity: Cracks can make nonwoven fabrics stronger, Journal of the Mechanics and Physics of Solids 77 (2015) 61 – 69.

[25] B. Sabuncuoglu, M. Acar, V. V. Silberschmidt, Parametric code for generation of finite-element model of nonwovens accounting for orientation distribution of fibres, International Journal for Numerical Methods in Engineering 94 (2013) 441–453.

[26] S. Michielsen, B. Pourdeyhimi, P. Desai, Review of thermally pointbonded nonwovens: Materials, processes, and properties, Journal of Applied Polymer Science 99 (2006) 2489–2496.

[27] R. Jubera, A. Ridruejo, C. Gonzlez, J. LLorca, Mechanical behavior and deformation micromechanisms of polypropylene nonwoven fabrics as a function of temperature and strain rate, Mechanics of Materials 74 (2014) 14 – 25.

[28] B. Sabuncuoglu, E. Demirci, M. Acar, V. V. Silberschmidt, Analysis of rate-dependent tensile properties of polypropylene fibres used in thermally bonded nonwovens, Journal of the Textile Institute 104 (2013) 965–971.

[29] B. Sabuncuoglu, M. Acar, V. V. Silberschmidt, Finite element modelling of thermally bonded nonwovens: Effect of manufacturing parameters on tensile stiffness, Computational Materials Science 64 (2012) 192 – 197.

[30] MSC-Software, Theory and User Information, 2016a.

[31] T. Belytschko, W. K. Liu, B. Moran, K. Elkhodary, Nonlinear Finite Elements for Continua and Structures, Wiley, 2013.

[32] F. Farukh, E. Demirci, B. Sabuncuoglu, M. Acar, B. Pourdeyhimi, V. V. Silberschmidt, Numerical modelling of damage initiation in low density thermally bonded nonwovens, Computational Materials Science 64 (2012) 112 – 115.

[33] M. N. Silberstein, C. L. Pai, G. C. Rutledge, M. C. Boyce, Elastic-plastic behavior of non-woven fibrous mats, Journal of the Mechanics of Physics of Solids 60 (2012) 295-318.

[34] C. T. Koh, D. G. T. Strange, K. Tonsomboon, M. L. Oyen, Failure mechanisms in fibrous scaffolds, Acta Biomaterialia 9 (2013) 7326 – 7334.

[35] A. Ridruejo, R. Jubera, C. Gonzalez, J. Llorca, Inverse notch sensitivity: Cracks can make nonwoven fabrics stronger, Journal of the Mechanics of Physics of Solids 77(2015) 61-69.

[36] A. Ridruejo, C. Gonzalez, J. Llorca, A constitutive model for the in-plane mechanical behaviour of nonwoven fabrics, International Journal of Solids and Structures 49 (2012) 2215-2229.

[37] A. Rawal, A. Paharia, V. Kumar, Enhancing the mechanical properties of virgin and damaged jute/polypropylene hybrid nonwoven geotextiles via mild alkali treatment of jute fibres, Textile Research Journal 88 (2018) 2132 – 2140.

GRAPHICAL ABSTRACT